THE ASTROPHYSICAL JOURNAL, 379:676–682, 1991 October 1

MODELS FOR LIGHT SCATTERING BY DUST AROUND HERBIG-HARO OBJECTS

ALBERTO NORIEGA-CRESPO
Astronomy Department, FM-20, University of Washington, Seattle, WA 98195
NURIA CALVET
Centro de Investigaciones de Astronomia, Apartado Postal 264, Mérida 5101-A, Venezuela
AND
KARL-HEINZ BÖHM
Astronomy Department, FM-20, University of Washington, Seattle, WA 98195
Received 1990 November 26; accepted 1991 April 9

ABSTRACT

Recent spectrophotometric observations of the Herbig-Haro 1–2 system by Solf and Böhm show in the position-velocity diagrams of Herbig-Haro 1 a faint broad blueshifted emission in front of it. The effect appears strongly in the [O I] λ6300/63 and [S II] λ6716/31 emission lines. We assume that this emission is produced by light scattering by dust in the preshock region. We present a series of theoretical position-velocity diagrams in [S II] λ6731, based on the single-scattering approximation. The models assume a spherical emitting source moving through a stationary gas cloud. The theoretical position-velocity diagrams with optical depths between $\sim$0.1 and 0.01 seem to account for the broad blueshifted emission and its integrated intensity.

Subject headings: radiative transfer — stars: circumstellar shells — stars: pre–main-sequence

1. INTRODUCTION

Herbig-Haro (hereafter HH) objects are associated with the strong supersonic collimated winds (jets) generated by pre–main-sequence stars (Mundt 1985, 1987). The interaction of the ejected matter and the surrounding medium is through shock waves, and therefore the emitted spectra resemble that of the recombination region behind a shock wave (Schwartz 1975). Their spectra are very bright in the neutral lines of [N I] λ5200, [O I] λ6300/63, and [C I] λ9823/49, as well as in the low excitation lines [S II] λ6716/31, among others. The hydrodynamic interaction takes place in the *working surface*, where wind material is abruptly decelerated and the environment is supersonically struck (e.g., Raga 1988; Hartigan 1989; Blondin, Fryxell, & Königl 1990). If the density of the jet is larger than that of the surrounding medium, then the flow looks like a *bow shock*, i.e., similar to that produced by a blunt obstacle in a supersonic flow (e.g., Raga 1988; Hartigan 1989). Some noteworthy exceptions to this kind of flow are, for instance, HH 43 (Böhm & Solf 1990) and HH 7–11 (Hartigan, Raymond, & Hartmann 1987; Solf & Böhm 1987).

Since HH objects are found in star-forming regions, it has been recognized for some time that dust scattering can be important in their environment and in the objects themselves. The presence of dust scattering has been inferred mostly from the measurement of linear polarization (see, e.g., Strom et al. 1985; Scarrot 1988; Scarrot & Warren-Smith 1988). Dust scattering has typically been detected in their surrounding medium (see, e.g., Strom et al. 1985, 1986), and in some cases in the HH objects' continuum emission (see, e.g., Strom, Grasdalen, & Strom 1974b; Strom, Strom, & Kinman 1974a; Schmidt & Miller 1979; Cohen & Schmidt 1981).

Recent observational results by Solf & Böhm (1991) have shown that interesting conclusions about the properties of the HH 1/HH 2 system can be drawn from the detailed spectroscopic study of dust scattered emission lines in the environment of this system. The system is believed to consist of bipolar jets originating in the young stellar object VLA 1 (Pravdo et al. 1985). In HH 1 the working surface of the jet shows a clearly observable bow shock (Choe, Böhm, & Solf 1985; Raga et al. 1988), whereas the working surface connected with HH 2 shows a much more complicated structure (see, e.g., Cantó & Rodríguez 1986) which is not yet fully understood. It is important to note that the axis of the flow in the jet and the HH 1/HH 2 system lies in the plane of the sky (Herbig & Jones 1981), and therefore the radial velocities are quite small but the radial velocity dispersions due to the bow shock structure are large, particularly in HH 1 (see, e.g., Böhm & Solf 1985).

Recently it has become possible to study the position-velocity (*p-v*) diagrams (spatially dependent line profiles) of strong emission lines in the preshock region, i.e., in front of the HH 1/HH 2 objects (Solf & Böhm 1991). These line profiles, especially in the preshock region of HH 1, show a rather large blueshift in addition to a large velocity dispersion, with centroid radial velocities of ~ -150 km s^{-1} and velocities in the blue wings of ~ -300 km s^{-1}, i.e., they differ drastically from the line profiles inside the HH objects. The best interpretation of these effects seems to be the following. The dust in front of HH object, which is essentially at rest with respect to the observer, "sees" strongly blueshifted radiation from the rapidly approaching HH object. This blueshifted line radiation is scattered toward the observer without any further change in Doppler shift (because the dust is essentially at rest). A similar effect seems to take place in the surrounding halo of the active galaxy M82 (see, e.g., Solinger & Markert 1975). Models of the light scattering by dust in the outflowing gas in M82, for instance, have been used to explain the observed Hα emission line polarization (see, e.g., Visvanathan & Sandage 1972; Solinger, Morrison, & Market 1977; Scarrot & Easton 1990). The dust in the outflowing gas in this case acts as "moving mirrors." For HH 1 we think that the "mirrors" are essentially at rest and the object is moving.

The "light scattering" effect in HH 1 is best seen in the [S II] λ6716/31 and [O I] λ6300/63 emission lines, while in other lines there seems to be also "in situ" line formation (see Solf & Böhm 1991 for details). If this scenario is correct, it has a number of important implications. It would be possible, at least in principle, to measure matter velocities perpendicular to the line of sight. Proper motions certainly also measure velocities in the plane of the sky (Herbig & Jones 1981, 1983), but in this case it is not obvious whether we really observe material motion or just the state of excitation moving through the material. In view of these facts it would be highly interesting to attempt a theoretical study of the process proposed above. In the present paper we shall attempt a first exploration of the problem using a number of rather drastic approximations in order to keep the problem reasonably simple. Specifically, we have calculated a series of theoretical *p-v* diagrams in the [S II] λ6731 emission line. The diagrams are generated from numerical radiative transfer models of single-scattering of photons emitted by a moving spherical source, which are scattered by the dust in a spherical static gas cloud.

We have concentrated on a small number of parameters, given our limited knowledge of the dust conditions around HH objects, and the available observations. In § 2, we describe the assumptions and techniques for the numerical models. In § 3, we present the result from the models and discuss their consequences. In § 4, we summarize our conclusions.

2. THE SCATTERING MODELS

2.1. *The Radiative Transfer*

In order to simplify the problem, we have approximated the HH object by a moving spherical light source. We consider a source of radius r_0, surrounded by a static spherically symmetric homogeneous cloud of radius r_c and density $n_{\rm H}$.

We assume that the emission line in the source (before the scattering process occurs) has an e^{-1} width described by a velocity $\boldsymbol{v}_0$. The whole source is moving with a velocity v_s. These assumptions are approximations. In reality different parts of the HH object have different hydrodynamic velocities which we simply approximate by a single velocity v_s plus an (isotropic) Gaussian velocity distribution. Our justification for this approach is the following. Most of the bow shock line emission comes from a rather limited spatial range near the stagnation region for which the velocity dispersion (along the direction of the jet flow) is only moderate. It is probably not too critical in which way the source velocity dispersion is approximated. The large width of the scattered line is primarily generated in the scattering process itself (see below). It is of course true that in the long run a detailed model of the emission-line scattering using a realistic HH object model as a radiation source should be calculated. This, however, would be a rather complex computation which, in view of our limited knowledge of the dust distribution near HH 1, may not yet be justified.

In the present paper the photon-scattering process has been included in its most simple form, in which each photon is scattered just once, i.e., the single-scattering approximation. The assumption is good as long as the optical depth (τ) is $\tau \leq 1$, for $\tau > 1$ the single-scattering approximation breaks down, and multiple-scattering must be included (Witt 1977). The radiative transfer method that we follow is similar to that of Calvet et al. (1990) in their study of scattered light around jets associated with HH objects.

The radiative transfer equation is solved in a spherical geometry where the radial and angular coordinates are generally r and $\mu = \cos\theta$, where θ is the angle between r and the ray direction (e.g., Mihalas 1978, p. 245). The method considers a set of parallel rays specified by an impact parameter p and a distance z along the ray measured from the source, in such a way that the radial coordinate is defined by $r = (p^2 + z^2)^{1/2}$ (e.g., Hummer & Rybicki 1971).

The source has a velocity $\boldsymbol{v}_s$ and subtends an angle θ with respect to the observer, such that $\boldsymbol{v}_s \cdot \boldsymbol{n} = v_s \cos\theta$, where $\boldsymbol{n}$ is a unit vector along the line of sight. The source emits an intensity $I_s^v = I_0\,[\exp-(v/\boldsymbol{v}_0)^2]$, where $\boldsymbol{v}_0$ is the velocity width (see above).

The photons emitted by the source are scattered by the dust in the cloud, and because of the source motion, the photons are Doppler-shifted by the velocity component in the direction toward each grain. If the cloud is static, i.e., with no very large internal motions, then photons in the direction of the motion are blueshifted, while in the opposite direction they are redshifted. The scattering properties of the dust grains can be specified by an albedo and a phase function (see § 2.2). The phase function depends on the scattering angle Θ measured with respect to the radial position of the grain and the line of sight (e.g., Witt 1977).

The transfer problem can be solved by considering different light rays and their behavior in two reference frames centered on the source. One frame (x, y, z) with z pointing toward the observer, and another one (x', y', z') with z' along the source velocity. A dust grain at position $\boldsymbol{r}$ receives from the source an intensity:

$$I_v(\boldsymbol{r}) = I_0\,e^{-\tau(\boldsymbol{r})}\,e^{[-(v-\boldsymbol{v}\cdot\hat{\boldsymbol{r}}/v_0)]^2}\,, \tag{1}$$

where I_0 is the source intensity and $\tau(\boldsymbol{r})$ is the optical depth along the radial direction $\boldsymbol{r}$ between the source and the grain, $\hat{\boldsymbol{r}}$ is a unit vector along $\boldsymbol{r}$, and $e^{-\tau(\boldsymbol{r})}$ is the attenuation suffered by the source intensity. The optical depth is given by

$$\tau(\boldsymbol{r}) = \int_{-\infty}^{\boldsymbol{r}} \chi_v\,d\boldsymbol{r}\,, \tag{2}$$

where χ_v is the extinction at velocity $\boldsymbol{v}$, and $\boldsymbol{v}\cdot\boldsymbol{r} = vz'$. The observer receives a grain scattering emissivity

$$\eta_v = \sigma_v \int \left(\frac{d\omega'}{4\pi}\right)\Phi(\Theta) I_v(\boldsymbol{r})\,, \tag{3}$$

where σ_v is the total scattering coefficient (see, e.g., Mihalas 1978, p. 30), Φ is the phase function, and $\Theta = \cos^{-1}(z/r)$, i.e., the angle between the incident and the scattered photon. The integral in equation (3) is carried over the solid angle subtended by the source $\pi(r_0/r)^2$. A simple analytical approximation to the phase function is given by Henyey & Greenstein (1941)

$$\Phi = \frac{1-g^2}{(1+g^2-2g\cos\Theta)^{3/2}}\,, \tag{4}$$

where g is the asymmetry factor. We can write then the transfer equation along each ray for a given (x, y) for the specific intensity I_v at velocity $\boldsymbol{v}$ as

$$\mu\frac{dI_v}{dz} = \eta_v - \chi_v I_v\,, \tag{5}$$

where η_v is the emissivity and $\mu = \cos\theta$. The transfer equation is solved for a normalized intensity $I_{v'} = I_v/I_0$, at each normalized velocity $\boldsymbol{v}' = \boldsymbol{v}/\boldsymbol{v}_0$ along each $(x/r_0, y/r_0)$ ray. If d is the distance to the source, then the observed flux is

$$F_{v'} = \int I_v \, d\omega = (r_0/d)^2 I_0 \int I_{v'} \, dx \, dy \; . \quad (6)$$

And finally the total flux of the line centered at frequency ν_0 is given by

$$F = \frac{1}{c}\left(\frac{r_0}{d}\right)^2 (I_0 \nu_0 v_0) \int dx \, dy \int I_{v'} \, dv' \; . \quad (7)$$

2.2. *The Dust Properties*

The probability that a photon becomes either absorbed or scattered by a dust grain depends on the photon's wavelength. This probability is measured by the albedo, a_λ, of the dust grain, which is a function of the wavelength (Lillie & Witt 1976). Thus larger values of a_λ imply a higher probability for the photon to be scattered than to be absorbed.

The pattern of the scattered radiation as a function of direction is measured by the phase function (e.g., Martin 1978, p. 58). We use the parametric form of the phase function developed by Henyey & Greenstein (1941) (see eq. [4]). In this case the phase function is determined by the asymmetric factor, g_λ, which is a parameter that measures the average cosine of the angle of the scattered light as a function of wavelength (Lillie & Witt 1976).

The values of a_λ and g_λ can be determined by comparing, for instance, the observed Galactic extinction curve with those produced by radiative transfer models. Such transfer models depend on the dust grain size distribution and their mixture (e.g., Mathis, Rumpl, & Nordsieck 1977; Draine & Lee 1984). From the compilation of the values of a_λ and g_λ carried on by Bruzual, Magris, & Calvet (1988), we find that in the "optical range," a_λ varies from 0.63 ± 0.15 at 3000 Å to 0.55 ± 0.10 at 7000 Å, while g_λ varies from 0.74 ± 0.05 at 3000 Å to 0.40 ± 0.05 at 7000 Å (e.g., Bruzual et al. 1988, Fig. 1). For our theoretical *p-v* diagrams, we have chosen values of $a_\lambda = 0.54$ and $g_\lambda = 0.42$, i.e., centered at the [S II] λ6731 wavelength.

2.3. *The Effect of the Optical Depth*

The optical depth for a cloud of density $n_{\rm H}$ and radius r_c is determined by equation (2). The integrated optical depth of the spherical cloud is then given by

$$\tau_\lambda = \kappa_\lambda n_{\rm H} r_0 \left(\frac{r_c}{r_0} - 1\right) , \quad (8)$$

where κ_λ is the dust extinction cross section per hydrogen atom (H), which relates the hydrogen density with the fraction of dust in the cloud. The radius of the source is r_0. The value of κ_λ depends on the extinction curve, and therefore, on the grain size distribution and the chemical mixture. For a power-law distribution of sizes a, $n(a) \propto a^{-3.5}$ with $0.005 < a < 0.25$ μm, and a graphite-silicate mixture (Mathis et al. 1977; Draine & Lee 1984), which reproduces quite well the observed "average" extinction curve (see, e.g., Savage & Mathis 1979, Table 2), κ_λ varies, for instance, from $\sim 7.0 \times 10^{-22}$ cm^2 H^{-1} at $\lambda = 4400$ Å, to $\sim 4.0 \times 10^{-22}$ cm^2 H^{-1} at $\lambda = 7000$ Å. For the [S II] λ6731 wavelength, we obtain and use $\kappa_\lambda = 4.6 \times 10^{-22}$ cm^2 H^{-1}. Although it has been generally assumed that a θ Orionis extinction curve holds for the HH 1/HH 2 surroundings (e.g., Brugel 1989), it seems quite possible that the "standard" curve could describe the extinction characteristics of the region (Böhm, Raga, & Binette 1991). The value of κ_λ in the optical wavelength range is very similar in either case.

Once we have selected the values of r_c, r_0, and κ_λ, there is a one-to-one relationship between the gas density and the optical depth. Thus a low density implies, for example, a small optical depth, a relative low number of scattering particles, and therefore, a low intensity for the scattered light.

The estimated values of the preshock density in the neighborhood of HH 1 range from 50 to 300 cm^{-3} (e.g., Böhm & Solf 1985). Models of the emitted spectra for the HH 1/HH 2 system by bow shocks give reasonable line intensity ratios for preshock densities of 100 cm^{-3} (Hartman & Raymond 1984) and 500 cm^{-3} (Hartigan et al. 1987). We found that to match the observed relative integrated intensity of the scattered light (see § 3.2 and Table 1) we required a cloud density of $n_{\rm H} \sim 750$ cm^{-3}. The theoretical *p-v* diagrams were calculated with this density value, which corresponds to an optical depth $\tau_\lambda \sim 0.03$ (see below).

2.4. *The Model Parameters*

The effect of the light scattering by dust appears more pronounced, as mentioned above, in HH 1 in the [O I] λ6300/63

TABLE 1

INTEGRATED RELATIVE INTENSITIES[a]

	τ_λ[c]					
ΔX[b]	1.0[e]	0.1[f]	0.03[g]	0.04[h]	0.01[i]	HH 1[d]
0–5	2.2×10^{-1}	2.1×10^{-2}	1.2×10^{-2}	1.5×10^{-2}	4.1×10^{-3}	1.2×10^{-2}
5–10	1.0×10^{-1}	1.0×10^{-2}	5.1×10^{-3}	1.4×10^{-2}	1.1×10^{-3}	1.1×10^{-2}
10–15	2.2×10^{-2}	2.2×10^{-3}	9.9×10^{-4}	9.4×10^{3}	2.1×10^{-4}	6.6×10^{-3}

NOTE.—$n_{\rm H}$ = density of the gas cloud in cm^{-3}; r_c = radius of the gas cloud in arcseconds.
[a] For $V_s = 200$ km s^{-1}.
[b] Distance from the source in arcseconds.
[c] Cloud optical depth.
[d] HH 1 estimated values.
[e] $n_{\rm H} = 2.5 \times 10^4$ and $r_c = 15.3$.
[f] $n_{\rm H} = 2.5 \times 10^3$ and $r_c = 15.3$.
[g] $n_{\rm H} = 7.5 \times 10^2$ and $r_c = 15.3$.
[h] $n_{\rm H} = 5.0 \times 10^2$ and $r_c = 28.5$.
[i] $n_{\rm H} = 2.5 \times 10^2$ and $r_c = 15.3$.

and [S II] λ6716/31 emission lines. In order to compare with the available spectroscopic observations (Solf & Böhm 1991), we select values representative of the HH 1 region. For a distance of $\sim$500 pc to the HH 1/HH 2 complex and a radius of $\sim$3″ for the "head" of HH 1, we obtain $r_0 \sim 2.25 \times 10^{16}$ cm. The radius of the cloud is assumed to be the observed size of the scattered light in the preshock region, i.e., $\sim$15″, or $r_c \sim 5 \times r_0$ (see Fig. 2). For the above parameters and a $\kappa_\lambda = 4.60 \times 10^{-22}$ cm^2 H^{-1} with a density $n_H = 750$ cm^{-3}, we obtain an optical depth $\tau_\lambda \sim 0.03$.

The velocity of the source has been estimated from both the proper motions and the emitted spectrum of the HH 1/HH 2 system. For HH 1F, the leading condensation of HH 1, has a total tangential velocity of 351 $\pm$ 48 km s^{-1} (see, e.g., Herbig & Jones 1981; Raga, Barnes, & Mateo 1990). The bow shock velocities deduced from the theoretical models used in the interpretation of the emitted spectra, however, are smaller than 300 km s^{-1}. The ratios of the forbidden emission lines and their spatial intensity distributions, for instance (Hartigan et al. 1987; Noriega-Crespo, Böhm, & Raga 1989), indicate shock velocities between 150 and 200 km s^{-1}. We have calculated theoretical *p-v* diagrams for four source velocities, $v_s = 150$, 200, 250, and 300 km s^{-1}. The theoretical *p-v* diagrams have identical dust parameters, i.e., $a_\lambda = 0.54$, $g_\lambda = 0.42$, and $\kappa_\lambda = 4.60 \times 10^{-22}$ cm^2 H^{-1}.

Another parameter to be selected is the velocity width of emitting source, v_0 (see eq. [1]). The assumption of a spherical emitting source does not take into account the more complex nature of most HH objects as "working surfaces" (Hartigan 1989; Blondin et al. al. 1990). Even under the simplifying assumption of HH 1 as a "bow shock" (Hartman & Raymond 1984; Raga 1985), there is a velocity distribution along the shock, with higher flow velocities near the "stagnation point" decreasing downstream along the "bow shock wings."

The line profile of HH 1 in Hα, for instance, has a full width at half-maximum (FWHM) of $\sim$84 km s^{-1} (e.g., Hartigan et al. 1987, Fig. 4B) with a total width of $\sim$300 km s^{-1}. Thus photons emitted from the "bow shock wings" have different velocities than those arising from the stagnation point," and therefore they are scattered by the dust according to their relative velocities.

A proper treatment of the "working surface" velocity and emission distributions is beyond the scope of this study. The effect of an intrinsic width of the emitting source has been included by selecting a Gaussian profile with $v_0 = 50$ km s^{-1}, which corresponds to FWHM $\sim$ 84 km s^{-1}.

Finally, in order to compare with the available observations of HH 1, we have convolved the theoretical *p-v* diagrams with a two-dimensional Gaussian. This convolution simulates the effect of a limited resolution in space and wavelength, The "Gaussian resolution" has a velocity dispersion of $\sigma_V \sim 33$ km s^{-1} equivalent to a FWHM $\sim$55 km s^{-1}, and a spatial dispersion of $\sigma_X \sim 0\farcs9$, which corresponds to a FWHM $\sim 1\farcs5$, in agreement with the data quoted by Solf & Böhm (1991).

From the measured proper motions and radial velocities of the different condensations in the HH 1/HH 2 complex (Herbig & Jones 1981), it is known that the axis of the motion of the system lies very close to the plane of the sky. Although we calculated *p-v* diagrams for various angles between 80° and 90° we found slightly better agreement of the theoretical centroid radial velocities with the observations for a 80° angle. The theoretical *p-v* diagrams shown here are calculated to this orientation.

3. RESULTS AND DISCUSSION

3.1. *The Morphology of the Position-Velocity Diagrams*

The observational *p-v* diagram in front of the optical component of HH1 is blueshifted and broad in velocity space (see Fig. 2). The total width is $\sim$300 km s^{-1}, with a centroid radial velocity between -100 and -150 km s^{-1}. The velocity width is very similar as a function of position, as wide close to the source ($X \sim 0''$) as it is farther away ($X > 10''$). The centroid radial velocity changes slightly as a function of position and is more blueshifted (more negative) away from the source.

The above features are essentially reproduced by the theoretical *p-v* diagrams. Figure 1 shows the diagrams for $v_s = 150$, 200, 250, and 300 km s^{-1}, labeled (*a*), (*b*), (*c*), and (*d*), respectively.

In Figure 2 we show a comparison between the theoretical *p-v* diagram with $v_s = 200$ km s^{-1} and that of HH 1 in the [S II] λ6716/31 emission line (Solf & Böhm 1991). The overall morphology is surprisingly similar, considering the many assumptions involved.

In the theoretical diagrams, the total velocity width increases as the source velocity increases, reaching velocities up to ~ -237, -300, -360, and > -425 km s^{-1}, for $v_s = 150$, 200, 250, and 300 km s^{-1}, respectively. The effect is expected

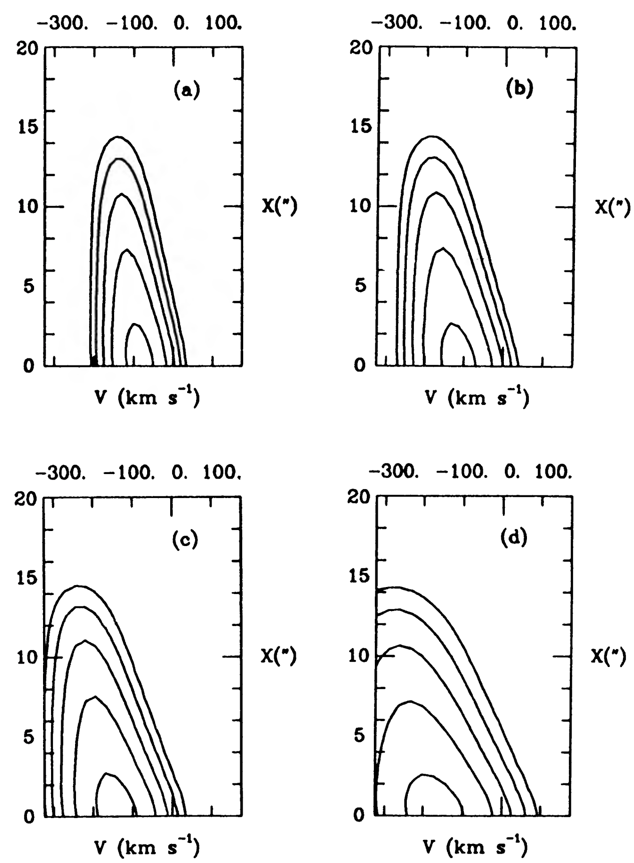

FIG. 1.—Theoretical position-velocity (*p-v*) diagrams for four source velocities $v_s = 150, 200, 250$, and 300 km s^{-1}, labeled (*a*), (*b*), (*c*), and (*d*), respectively. The *p-v* diagrams have been calculated with identical dust parameters, i.e. $a_\lambda = 0.54$, $g_\lambda = 0.42$, and $\kappa_\lambda = 4.60 \times 10^{-22}$ cm^2 H^{-1}, for $\lambda = 6731$ Å. The velocity and position axis are centered in the source velocity and position. The contours represent the intensity of the scattered light in the preshock region, i.e., ahead of the HH object. The intensity contour levels are drawn in factors of 2 (see text for details).

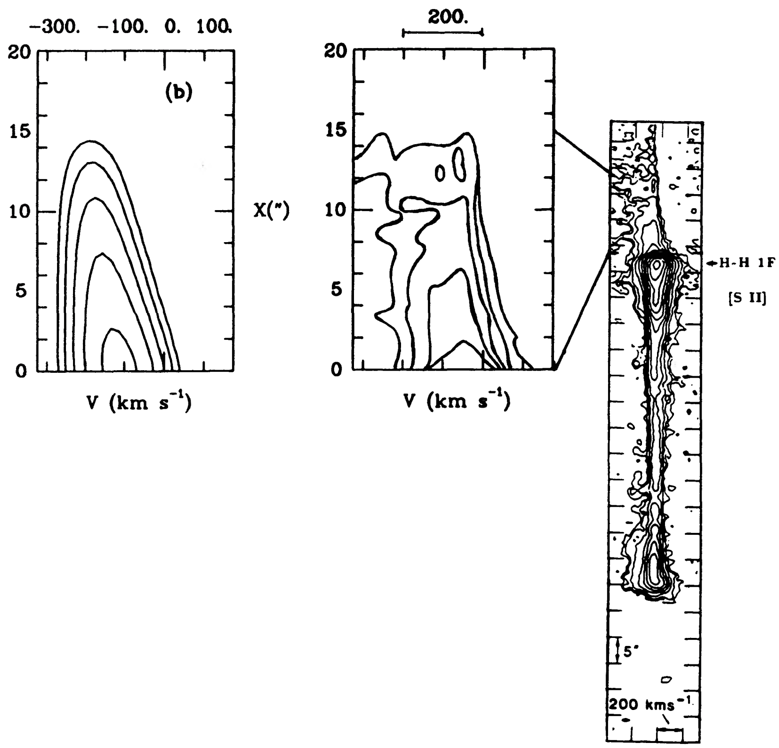

FIG. 2.—A comparison between the theoretical position-velocity diagram of the scattered light with a source velocity of $v_s = 200$ km s^{-1}, and that obtained from HH 1 (Solf & Böhm 1991) in the [S II] λ6716/31 emission line. In the observed position-velocity diagram is marked the position of HH 1F, the brightest optical condensation in HH 1.

from the scattering process, since for higher source velocities the dust receives photons which are more blueshifted. The centroid radial velocity, in front of the source ($X = 0$), becomes more negative as the source velocity increases, with values of ~ -100, -130, -170, and -200 km s^{-1} reached for $v_s = 100$, 200, 250, and 300 km s^{-1}, respectively (see Fig. 1).

The theoretical *p-v* diagrams seem to have a more tapered appearance than in HH 1. The radial velocity centroid becomes more negative more rapidly, as a function of position, than in the observations. The displacement is such that it gives an almost "trapezoidal" form to the theoretical *p-v* diagrams. This appearance of the theoretical diagrams could be partially due to the assumed sphericity of the surrounding cloud. The dust near the source essentially receives and scatters radiation from all relative velocities, this creates a broad component of scattered light near the source. Near the edge of the cloud, however, because of its spherical shape, only scattering angles of $\sim 90°$ are possible. In this zone the dust "sees" photons which show almost the full velocity of the moving source. Therefore, at larger distances from the source the emission becomes more narrow and strongly blueshifted, resulting in a more "trapezoidal" appearance of the *p-v* diagram. Thus the difference between the theoretical and the observed *p-v* diagrams may be indicating a departure from the spherical symmetry in the region surrounding HH 1.

3.2. *The Intensity of the Scattered Light*

As mentioned above, we expect the intensity of the scattered light to be determined by number of scattering particles and therefore to be different for different gas cloud densities (optical depths). In order to compare with the observations of HH 1, we have calculated the spatial intensity distributions and the integrated intensities for three different gas densities. We have assumed a source moving at $v_s = 200$ km s^{-1}, which produces a *p-v* diagram similar to that of HH 1 (see Fig. 2).

We have integrated the theoretical *p-v* diagrams over the cross section of the cloud (or source) as a function of position along the axis of asymmetry to obtain the spatial intensity distribution. The distribution for different optical depth models $\tau_\lambda = 1.0$, 0.1, and 0.01 (i.e., $n_H = 2.5 \times 10^4$, 2.5×10^3, and 2.5×10^2 cm^{-3}, respectively) are shown in Figures 3*a* and 3*b*. The effect of a narrow slit has been taken into account. In the models, however, the slit width is limited by the size of the source, i.e., $2 \times r_0 \sim 6''$, which is approximately 4 times the size of the slit ($\sim 1''.4$) used by Solf & Böhm in their spectroscopic observations.

Figure 3*a* shows the spatial distribution of the scattered light ahead of the source. The relative distance is measured, with respect to the edge of the source, in arcseconds. Figure 3*b* shows the spatial distributions of the respective sources. The theoretical sources distributions have been displaced to compare them with "working surface" or "bow shock" of HH 1.

Although both theoretical and observed sources have a total extension of $\sim 5''$, the model has a somewhat sharper peak (see Fig. 3). The distinct peak values of the source distributions are a result of the different attentuation that they suffered as they are seen, respectively, through clouds at different optical depths.

The integration of the spatial intensity distribution perpendicular to the symmetry axis ("along the line of sight") provides a measurement of the integrated intensity. We have taken the ratio of the integrated intensity of the scattered light with respect to that of the source, for each optical depth. We have

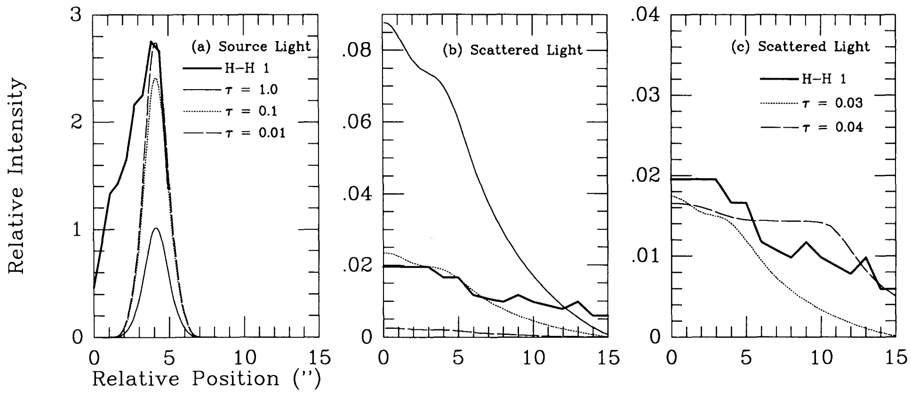

FIG. 3.—(*a*) The spatial intensity distributions for three emitting sources derived from the theoretical *p-v* diagrams compared with that of HH1 (*thick solid line*). The distributions correspond to three different optical depths, $\tau_\lambda = 1.0$ (*thin solid line*), 0.1 (*dotted line*), and 0.01 (*dashed line*), i.e., $n_H = 2.5 \times 10^4$, 2.5×10^3, and 2.5×10^2 cm^{-3}, respectively (for $r_c \sim 15''$). The relative position is measured (in arcseconds) with respect to the lowest intensity point in HH 1. The theoretical distributions have been shifted to compare their widths. (*b*) The corresponding spatial intensity distributions for the scattered light in the preshock region. The relative position is measured with respect to the edge of the source. (*c*) The spatial intensity distributions for two models with similar optical depths, but different r_c and n_H for the scattering region. The dotted line corresponds to $\tau_\lambda \sim 0.03$, $n_H = 750$ cm^{-3} and $r_c \sim 15''$; the dashed line corresponds to $\tau_\lambda \sim 0.04$, $n_H = 500$ cm^{-3}, and $r_c \sim 28''.5$. Their integrated intensities are given in Table 1.

taken the ratio of scattered light to the source at three linear intervals along the symmetry axis, i.e., 0″–5″, 5″–10″, and 10″–15″. A similar calculation was carried for HH 1, and for the $\tau_\lambda \sim 0.03$ model. The results are shown in Table 1.

The determination of the observed integrated values of the scattered light can be affected by light contamination from the source (near to it) and the background subtraction (away from it). Despite these effects, the values for the first interval (0″–5″) for $\tau_\lambda = 0.1$–0.01 are comparable to those calculated for HH 1. The value for $\tau_\lambda \sim 0.03$ is identical. In the intervals farther away from the source, the differences between the theoretical and observed values is somewhat greater, due to the behavior of the intensity distributions. The theoretical spatial intensity distributions decrease somewhat more rapidly than that observed in HH 1. For $\tau_\lambda \sim 0.03$ ($n_H \sim 750$ cm^{-3}), the integrated values are ~ 2 times smaller than those of HH 1, in the second (5″–10″) interval.

In comparing with the observations of HH 1, we have assumed that the size of the scattering cloud in the theoretical *p-v* diagrams is determined by the size of the observed scattering region. In principle, it is possible to calculate theoretical *p-v* diagrams for different sizes of scattering cloud or the gas density. These models, however, must be constrained still by the morphology of the *p-v* diagram, the spatial intensity distribution and the integrated intensities.

We have calculated the intensity distribution of the scattered light for a series of models for different values of r_c and n_H, maintaining the optical depth constant (see eq. [8]). We assumed an optical depth of $\tau_\lambda \sim 0.03$, as determined by the initial models. In Fig. 3*c*, we present, as an example, the spatial intensity distribution for a scattering cloud twice as large as the previous models. The parameters for this model are $\tau_\lambda \sim 0.04$, $n_H = 500$ cm^{-3}, and $r_c \sim 28''.5$ (see Table 1). We include for comparison the distributions from the model with $\tau_\lambda \sim 0.03$, $n_H \sim 750$ cm^{-3}, and $r_c \sim 15''$ (both models with $v_s = 200$ km s^{-1}), and that observed in HH 1. The spatial distribution for a larger r_c is slightly flatter than the observations, but still fairly similar. The gas density (~ 500 cm^{-3}) was chosen as to reproduce the observed integrated intensities (see Table 1). A scattering cloud twice as large as the previous models, with a lower density, is also consistent with the available observations of HH 1.

4. CONCLUSIONS

We have calculated a series of numerical models of the light scattering by dust around a moving object, applied in particular to Herbig-Haro objects. This study is motivated by the recent spectroscopic results obtained by Solf & Böhm (1991) of the HH 1/HH 2 system. They found that the *p-v* diagrams of HH 1 in the [O I] λ6300/63 and [S II] λ6716/31 emission lines show very extended blueshifted wings in the preshock region. We have interpreted this emission as scattering of the light of the moving HH 1 object by the surrounding dust. The bright "working surface or bow shock" acts as a moving emitting source, and its photons are "seen" blueshifted by the dust in front of it. The dust is essentially at rest with respect to the object and scatters the blueshifted photon toward the observer. In order to test this hypothesis, we have calculated a series of theoretical *p-v* diagrams based on the single-scattering approximation. The models assumed an emitting spherical source that moves in a spherical homogeneous gas-dust cloud of constant density at rest. The *p-v* diagrams assumed dust parameters and physical characteristics which resemble those of the HH 1/HH 2 region. We have shown in Figures 1 and 2 the *p-v* diagrams for four source velocities (150, 200, 250, and 300 km s^{-1}). We found that the light scattering by dust around a moving source can produce extended blueshifted wings of ~ -300 km s^{-1}, with centroid radial velocities between ~ -100 to -150 km s^{-1}, as it is observed in HH 1 (Solf & Böhm 1991).

The single-scattering model with $\tau_\lambda \sim 0.03$ and $v_s \sim 200$ km s^{-1} produces a theoretical *p-v* diagram similar, in form and characteristics, to that observed in HH 1. The scattering models provide a simple mechanism to understand the faint broad blueshifted emission. A source velocity of 200 km s^{-1} is in agreement with other velocity determinations, e.g., from the emission-line ratios or their spatial intensity distributions. The *p-v* diagrams with larger source velocities (>250 km s^{-1}) display a significant contribution from the fast blueshifted photons, which gives them a more "trapezoidal" form than that of HH 1. The appearance of these high-velocity *p-v* diagrams, however, can be partially due to the assumed sphericity of the surrounding cloud. The difference between the shape of these models and the observations may reflect a departure from the assumed spherical symmetry in the HH 1 region.

We have roughly estimated the relative integrated intensities of the scattered light and the source. We found that the models with $n_H \sim 750$ cm^{-3}, or equivalently with $\tau_\lambda \sim 0.03$, have integrated intensities very close to the observations over similar length intervals. The integrated values farther away from the source are, however, slightly smaller. This is partially due to the more rapid decline of the theoretical spatial intensity distributions, and to the inherent difficulties of background subtraction in the observations at such a low-intensity level. A preshock gas density of $n_H \sim 750$ cm^{-3}, is slightly larger than what has been determined in HH 1 (e.g., Böhm & Solf 1985) by about a factor of 3. The gas density can be reduced by keeping τ_λ constant and increasing the size of scattering cloud. Calculations for different cloud sizes are also important because we do not know, a priori, which cloud radius is appropriate. We calculated, as an example, the spatial intensity distribution for a model with $\tau_\lambda \sim 0.04$, $n_H = 500$ cm^{-3} and $r_c \sim 28''.5$. The size of the scattering region is approximately twice as large as the previous models (see Table 1). We found that the spatial intensity distribution and its integrated values are still consistent with the available observations of HH 1.

An additional important test of the dust scattering model of line formation near HH objects would be the measurement of linear polarization. Broad-band polarization measurements in the HH 1/HH 2 diffuse regions have indeed been done by Strom et al. (1985). Polarization measurements in individual lines will be much more difficult, especially in view of the fact that the intensity at 10" from the source is only ~0.5% of the intensity in the HH 1 object itself. Since, however, the expected polarization is high, an attempt of detecting it may be worthwhile in the near future.

The observational background which led to this theoretical study is due to J. Solf. We thank him for very helpful discussions. We thank Bill Waller for his comments on M82. N. C. and A. N.-C. thank the PITA members of Luc Binette, Jorge Cantó, and Alex Raga for their comments. We thank the anonymous referee for her/his careful reading of the manuscript and for her/his comments on the intensity of the scattered light. K. H. B. and A. N.-C.'s research has been supported by the NSF grant AST-8918458.

REFERENCES

Blondin, J. M., Fryxell, B. A., & Königl, A. 1990, ApJ, 360, 370
Böhm, K. H., Raga, A. C., & Binnette, L. 1991, PASP, in press
Böhm, K. H., & Solf, J. 1985, ApJ, 294, 533
———. 1990, ApJ, 348, 297
Brugel, E. W. 1989, in Low Mass Star Formation and Pre-Main Sequence Objects, ed. B. Reipurth (Garching bei München: ESO), 311
Bruzual, A., Magris, C., G., & Calvet, N. 1988, ApJ, 333, 673
Calvet, N., Cantó, J., Raga, A. C., Lizano, S., & Binette, L. 1990, Rev. Mexicana Astr. Af., submitted
Cantó, J., & Rodríguez, L. F. 1986, Rev. Mexicana Astr. Af., 13, 57
Choe, S.-U., Böhm, K. H., & Solf, J. 1985, ApJ, 288, 338
Cohen, M., & Schmidt, G. D. 1981, AJ, 86, 1228
Draine, B. T., & Lee, H. M. 1984, ApJ, 285, 89
Hartigan, P. 1989, ApJ, 339, 987
Hartigan, P., Raymond, J., & Hartmann, L. 1987, ApJ, 316, 323
Hartmann, L., & Raymond, J. 1984, ApJ, 276, 560
Henyey, L. G., & Greenstein, J. L. 1941, ApJ, 93, 70
Herbig, G. H., & Jones, B. F. 1981, AJ, 86, 1232
———. 1983, AJ, 88, 1040
Hummer, D., & Rybicki, G. 1971, MNRAS, 152, 1
Lillie, C. F., & Witt, A. N. 1976, ApJ, 267, 119
Martin, P. G. 1978, Cosmic Dust (Oxford: Oxford Univ. Press)
Mathis, J. S., Rumpl, W., & Nordsieck, K. H. 1977, ApJ, 217, 425
Mihalas, D. 1978, Stellar Atmospheres (2d ed.; San Francisco: Freeman)
Mundt, R. 1985, in Protostars and Planets, Vol. 2, ed. D. C. Black & M. S. Matthews (Tucson: Univ. of Arizona Press), 414
———. 1987, in IAU Symposium 122, Circumstellar Matter, ed. I. Appenzeller & C. Jordan (Dordrecht: Reidel), 147
Noriega-Crespo, A., Böhm, K. H., & Raga, A. C. 1989, AJ, 98, 1388
Pravdo, S. H., Rodríguez, L. F., Curiel, S., Cantó, J., Torrelles, J. M., Becker, R. H., & Sellgren, K. 1985, ApJ, 293, L35
Raga, A. C. 1985, PhD thesis, University of Washington
———. 1988, ApJ, 335, 825
Raga, A. C., Barnes, P. J., & Mateo, M. 1990, AJ, 99, 1919
Raga, A. C., Mateo, M., Böhm, K. H., & Solf, J. 1988, AJ, 95, 1783
Savage, B. D., & Mathis, J. S. 1979, ARAA, 17, 73
Scarrott, S. M. 1988, MNRAS, 231, 1055
Scarrott, M., & Eaton, N. 1990, Gemini, 30, 17
Scarrott, S. M., & Warren-Smith, R. F. 1988, MNRAS, 232, 725
Schmidt, G., & Miller, J. S. 1979, ApJ, 234, L191
Schwartz, R. D. 1975, ApJ, 195, 631
Solf, J., & Böhm, K. H. 1987, AJ, 93, 1172
———. 1991, ApJ, 375, 618
Solinger, A. B., & Markert, T. 1975, ApJ, 197, 309
Solinger, A., Morrison, P., & Markert, T. 1977, ApJ, 211, 707
Strom, K. M., Strom, S. E., & Kinman, T. D. 1974a, ApJ, 191, L93
Strom, K. M., Strom, S. E., Wolff, S., Morgan, J., & Wenz, M. 1986, ApJS, 62, 39
Strom, S. E., Grasdalen, G. L., & Strom, K. M. 1974b, ApJ, 191, 111
Strom, S. E., Strom, K. M., Grasdalen, G. L., Sellgren, K., Wolff, S., Morgan, J., Stocke, J., & Mundt, R. 1985, AJ, 90, 2281
Visvanathan, N., & Sandage, A. 1972, ApJ, 176, 57
Witt, A. 1977, ApJS, 35, 1